Analysis of the operating mechanism and parameter optimization of the upright conveying device for reed harvesters

Jicheng Huang[1,2], Bin Zhang[1,3], Kunpeng Tian[1,2], Senlin Mu[1], Fanting Kong[1], Zhongqiu Mu[1], Weijie Shen[4*], Cheng Shen[1,3*]

(1. *Nanjing Institute of Agricultural Mechanization, Ministry of Agriculture and Rural Affairs, Nanjing 210014, China*;
2. *College of Mechanical and Electrical Engineering, Hohai University, Changzhou 213022, China*;
3. *School of Mechanical Engineering, Southeast University, Nanjing 211189, China*;
4. *Zhejiang Technical Institute of Economics, Hangzhou 310018, China*)

Abstract: To investigate the operational mechanism and quality improvement strategies of a reed upright conveying device, first, the structural design was completed, and a force analysis of the conveying process was conducted. A rigid-flexible coupling simulation model of reed stalks and the conveying mechanism was then employed to examine the effects of the structural parameters of the conveying chain links on the maximum contact force exerted on the reed stalks and to identify the optimal parameter combination. High-speed photography experiments were carried out during the conveying process to capture the motion states and trajectories of the reed stalks, elucidating the causes of stalk breakage and blockages. Subsequently, response surface experiments were conducted to investigate the primary factors influencing upright conveying quality. Mathematical models for predicting damage rate and conveying rate were established, and the effects of various factors on these indicators were analyzed. Multi-objective optimization of the regression models was performed based on practical production requirements, yielding an optimal parameter combination: transverse conveying speed of the chain at 1.1 m/s, speed ratio of 1.2, and upper conveying chain position at 1.37 m. Experimental results indicated a damage rate of 11.90% and a conveying rate of 95.11%, meeting the operational requirements for mechanized reed harvesting and conveying. These findings provide fundamental theoretical data for the development of reed harvester conveying components and the selection of operational parameters.

Keywords: reed harvester, upright conveying device, operating mechanism analysis, parameter optimization, high-speed photography

DOI: 10.25165/j.ijabe.20251803.9704

Citation: Huang J C, Zhang B, Tian K P, Mu S L, Kong F T, Mu Z Q, et al. Analysis of the operating mechanism and parameter optimization of the upright conveying device for reed harvesters. Int J Agric & Biol Eng, 2025; 18(3): 135–144.

1 Introduction

Reed, a perennial herbaceous plant of the Poaceae family, has a wide range of applications. It serves as a high-quality raw material for papermaking, and is an ideal source for composite materials, biochar, and other industrial uses[1-4]. Additionally, reed possesses significant ecological value, playing a vital role in climate regulation, silt deposition, erosion prevention, algae growth inhibition, wastewater purification, and flood control[5,6]. However, most reed grows in wetlands and marshes, characterized by waterlogged and muddy conditions. Combined with challenges such as wind, pest damage, and vine entanglement, these factors result in stalks being interwoven and lodged, making manual harvesting highly difficult under harsh and demanding conditions. Mechanized harvesting of reed is therefore a prerequisite for its efficient utilization as a resource. Domestic harvesters in China lack versatility and technological maturity. Most models are still in the prototype testing phase. In some regions, modified reaping machines are used to address harvesting issues partially, but they suffer from limitations such as narrow cutting widths, unstable harvesting quality, and low operational efficiency, necessitating further improvement and optimization[7-11]. While foreign harvesting machinery for reed is relatively advanced, their process generally involves cutting the reeds, immediately crushing and compressing them into square or round bales, which consumes a lot of energy. This method is only suitable for harvesting reed varieties with thin, short stems and high growth density, like those found in northern China. It is not applicable to harvesting reed varieties with thicker, taller stems and relatively lower growth density in southern China. Moreover, foreign harvesting machinery is typically priced higher, which reduces the willingness of domestic reed farmers to purchase it from an economic standpoint[12-14].

The harvesting process of reed primarily involves cutting, conveying, and either laying or baling for collection. Among these,

Received date: 2025-01-23 **Accepted date:** 2025-05-20

Biographies: Jicheng Huang, Associate Professor, research interest: agricultural mechanization, Email: huangjicheng@caas.cn; **Bin Zhang**, Professor, research interest: agricultural engineering, Email: xtsset@hotmail.com; **Kunpeng Tian**, Associate Professor, research interest: agricultural mechanization, Email: tiankp2005@163.com; **Senlin Mu**, Professor, research interest: agricultural engineering, Email: musenlin@caas.cn; **Fanting Kong**, Assistant Professor, research interest: agricultural engineering, Email: kongfanting1989@163.com; **Zongqiu Mu**, research assistant, research interests: agricultural engineering, Email: muzhongqiu@caas.cn.

***Corresponding author: Weijie Shen**, Lecturer, research interest: vehicle engineering, Zhejiang Technical Institute of Economics, No.66 Xuezheng Street, Qiantang District, Hangzhou 310018, China. Tel: +86-15957199805, Email: 240056@zjtie.edu.cn; **Cheng Shen**, Associate Professor, research interest: agricultural mechanization engineering, Nanjing Institute of Agricultural Mechanization, Ministry of Agriculture and Rural Affairs, No.100 Liuying, Xuanwu District, Nanjing 210014, China. Tel: +86-25-84346078, Email: shencheng@caas.cn.

stalk conveying is a critical step in the harvesting process. However, existing conveying technologies for tall-stalk crops offer limited applicability to reed stalks. This is primarily due to the unique biomechanical properties of reed, characterized by tall and brittle stalks that are prone to breaking during cutting and conveying. These challenges often result in stalk breakage and blockages during conveying. The root cause lies in the lack of research on key aspects, including the biomechanical and mechanical property models of reed stalks, the appropriate mechanical interaction modes and parameters for conveying mechanisms, and the operational quality mechanisms. Consequently, issues such as frequent stalk breakage, blockages, and low reliability during mechanized harvesting of reed remain unresolved.

To address the aforementioned issues and improve the operational quality of the conveying mechanism and the overall performance of reed harvesters, the authors previously developed a reed harvester featuring a conveying device capable of upright clamping and transporting reed stalks[15]. However, its adaptability and operational performance require further enhancement. This study focuses on the mechanical characteristics of the upright conveying process, the rigid-flexible coupling multi-body dynamic model of the stalk-conveying mechanism, and multi-objective optimization of conveying quality. The aim is to derive an optimized design scheme for the structural and operational parameters of the upright conveying mechanism for reed. The findings are expected to provide valuable insights for advancing mechanized reed harvesting technology and optimizing conveying mechanisms.

2 Structure and working principle

2.1 Structure of the upright conveying device

The reed harvester discussed in this study utilizes a dual-chain upright conveying mechanism designed to stably and smoothly transport reed stalks, cut by the cutter, to one side of the header. This ensures that no tilting, breakage, or blockages occur during the conveying process. The mechanism primarily consists of components such as a stalk feeding star wheel, conveying chains, compression springs, and a guiding plate, as shown in Figure 1. The upper and lower conveying chains are connected via universal joints to achieve synchronized operation of both chains.

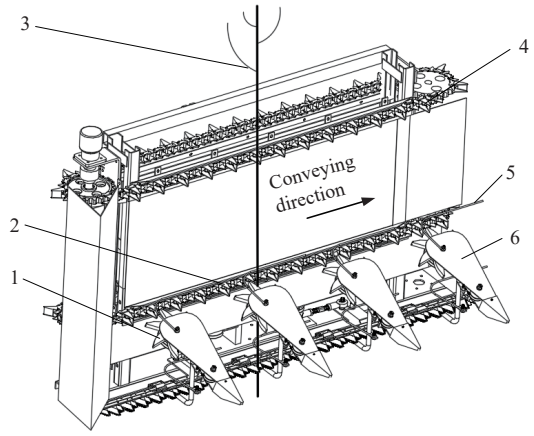

1.Feeding star wheel; 2.Lower conveying chain; 3.Reed plant; 4.Upper conveying chain; 5.Compression spring; 6.Stalk-guiding plate

Figure 1 Schematic diagram of reed upright conveying device structure

The upright conveying process essentially involves the clamping action formed by the conveying chain and compression springs, which apply pressure to the reed stalks. The stalks are driven forward by the chain links and the crop-guiding star wheel. The structure of the clamping conveying chain designed in this study is shown in Figure 2. It primarily consists of long chain links, standard chain links, and pressing plates. This chain is a modified version of a conveying chain used in agricultural machinery[16,17], characterized by its ability to evenly clamp and transport reed stalks. The long chain links play a role in driving the rotation of the stalk-guiding star wheel in the guiding mechanism, directing the stalks into the clamping conveying device. Together, the long chain links and standard chain links ensure secure clamping of the stalks, while the pressing plates serve to constrain the chain's position within the guide rail.

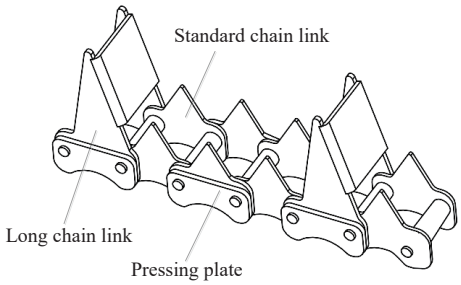

Figure 2 Schematic diagram of conveying chain structure

2.2 Working principle of the upright reed conveying test bench

To further investigate the upright conveying process and optimize the conveying mechanism of the reed harvester, a upright conveying test bench was constructed, as shown in Figure 3. The test bench primarily consists of a feeding device, cutting device, upright conveying device, stalk-guiding device, and control platform. During operation, reed plants are guided toward the stalk-guiding device by the feeding device. With the assistance of the stalk-guiding device, the plants within the working width are lifted and directed into the cutting device for cutting. The cut stalks are then horizontally conveyed in an upright position to one side of the header by the combined action of two sets of upper and lower chain conveying mechanisms and compression springs. Once released from the transverse conveying chain, the stalks are laid down on one side of the test bench under the combined effects of their weight and the inertial force generated by the transverse conveying chain, completing the operation process.

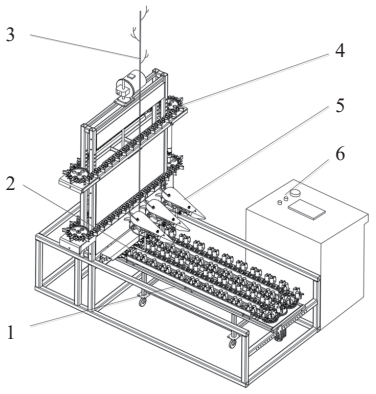

1.Feeding device; 2.Reciprocating double-action cutter device; 3.Reed plant; 4.Upright conveying device; 5.Stalk-guiding device; 6.Control platform

Figure 3 Structural diagram of reed upright conveying test bench

3 Force and simulation analysis of the conveying process

3.1 Force analysis of the conveying process

The lateral transportation conditions for reed plants refer to the requirements that must ensure that the plants remain stable and do not experience significant tilting or flipping during the transportation process after being cut. After the reed plants enter the upright conveying device, they are clamped and compressed in the gap formed between two adjacent chain links of the clamping conveying chain and the compression springs. The forces acting on the stalks within the conveying channel are complex, primarily including the tooth forces from the upper and lower clamping conveying chains, the friction forces between the stalks and the baseplate or side plates, and the interaction forces between stalks. These forces collectively influence the final conveying performance. To simplify the analysis, it is assumed that the plants experience minimal compressive deformation within the transportation channel. An analysis of the forces exerted on the stalks during conveying, particularly on the conveying chain and at the clamping points, is conducted, as illustrated in Figures 4 and 5.

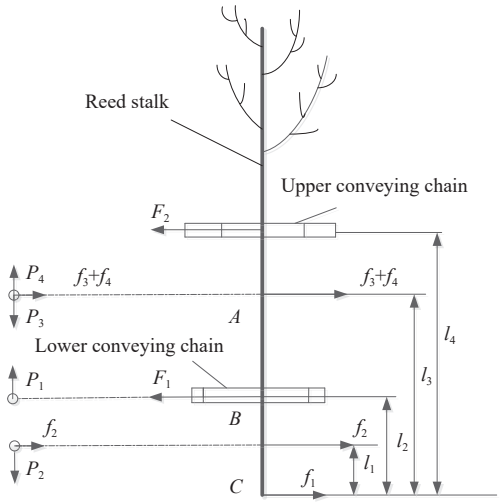

Figure 4 Force analysis of reed stalks on the conveying chain

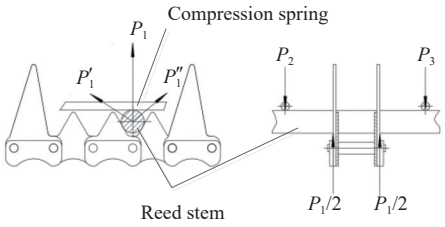

Figure 5 Force analysis of reed stalks at the clamping position

The mechanical relationship of the transverse stalk conveying should satisfy the following condition[18-20]:

$$F_1 + F_2 \geq f_1 + f_2 + f_3 + f_4 \tag{1}$$

In the equation: F_1 and F_2 represent the forces exerted by the chain teeth on the reed stalks; f_1 is the frictional resistance between the baseplate and the stalks; f_2 is the frictional resistance between the lower side plate and the stalks; f_3 is the frictional resistance between the upper side plate and the stalks; and f_4 is the interaction force between the stalks.

The conditions for no stalk detachment or rotation should satisfy the following: the forces in the horizontal and upright directions must be in equilibrium, and the moment at point C must be Mc=0.

$$\begin{cases} \sum M_1 = F_1 \cdot l_2 + F_2 \cdot l_4 - f_2 \cdot l_1 - (f_3 + f_4) \cdot l_3 = 0 \\ \sum M_2 = P_2 l_1 - P_1 l_2 + (P_3 - P_4) \cdot l_3 = 0 \end{cases} \tag{2}$$

In the equation: P_4 represents the support force of the side plate; P_2 and P_3 are the pressures exerted by the compression springs on the reed stalks; P_1 is the support force of the chain; and l_1, l_2, l_3, and l_4 are the vertical distances from the points of action of forces f_2, F_1, f_3, f_4, and F_2 to the baseplate.

The measured height of the reed stalks ranges from 3000 mm to 4500 mm. According to the *Manual of Agricultural Machinery*, the initial design parameters are as follows: the distance from the bottom plate to the lower conveying chain is 450 mm, the distance from the bottom plate to the upper conveying chain is 1350 mm, and the header height is 1540 mm.

3.2 Simulation analysis of the conveying process

3.2.1 Establishment of the dynamics model for the conveying process

A three-dimensional model of the reed stalk was created using Croe software, with the dimensional and shape parameters determined based on field survey data. The model has a height of 3500 mm, a taper of 0.003, a root outer diameter of 12.80 mm, and a wall thickness of 1.76 mm. After constructing the 3D model of the reed stalk, it was saved in Parasolid format. Importing the Parasolid file directly into ADAMS software would result in a rigid body model, which would not undergo any deformation during the simulation, failing to reflect real-world bending or other deformations. Therefore, it is necessary to first establish a flexible body model for the stalk. ADAMS offers three methods for creating flexible body models: (1) Discrete flexible link; (2) Modal neutral file generated by meshing in ANSYS or other finite element software; (3) Direct meshing using the ADAMS/AutoFlex module to generate a modal neutral file. Among these three methods, the modal neutral file most accurately reflects the mechanical properties[21,22]. Therefore, this study uses ANSYS to create the flexible body model for the reed stalk. The mechanical parameters of the stalk are: mass density of 650 kg/m^3, Young's modulus of 75.52 MPa, and Poisson's ratio of 0.3. The Solid185 element is chosen as the material element, and meshing is performed using the Smart Size method. For computational accuracy and simulation efficiency, the mesh precision is set to 5, resulting in 4 249 495 elements and 832 005 nodes. After meshing, the stalk model is exported as an Adams-readable MNF file using the "Export to Adams" function.

For the subsequent optimization of the conveying chain link structure parameters, the conveying chain model is constructed in ADAMS using a parametric modeling approach. In the actual stalk conveying process, the reed stalks that are tightly compressed are typically situated between two adjacent links and do not make contact with the other links of the chain. Therefore, the chain model can be simplified. Each set of conveying chains is simplified into six chain links, with each link accurately constructed using seven point positions. The simplified models of the upper and lower sets of conveying chains require 84 points in total. To ensure the accurate placement of these 84 points, the coordinates of the points are created in Excel and imported into the ADAMS/Views table editor, as shown in Figure 6.

To facilitate the subsequent chain link modeling, the "rename" command is used to sequentially modify the names of the points.

The polygon plate tool is then used to set the thickness and radius, connecting seven position points to complete the construction of a single chain link model. The same method is applied to construct the chain model. To allow for parameterized changes in the tooth shape angle and chain link thickness, design variables for *chixingjiao* and *houdu* must be created.

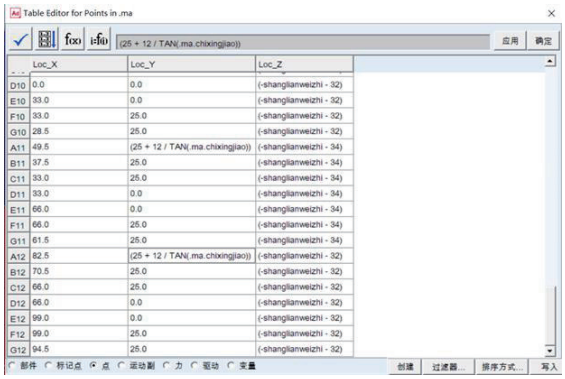

Figure 6 Parametric model data of chain links

The motion of the conveyor chain during the conveying process can be viewed as a combination of uniform linear motion in the transverse direction and uniform linear motion in the direction of the machine's forward movement, while the compression spring can be considered as moving uniformly in the forward direction. The simulation model requires the addition of numerous kinematic pairs and driving components. If manually added, this would not only be time-consuming and labor-intensive, but also prone to errors in the selection of the position or direction of the kinematic pairs. To address this, the "constraint create joint Planar" and "constraint create joint Translational" commands are used to automatically and accurately add kinematic pairs to each component. The marker points for the kinematic pairs on the components are associated with the component's center of mass using the "loc_relative_to" command. This approach is designed to prevent the separation of kinematic pairs and components due to position changes during subsequent parametric simulations.

After adding the kinematic pairs, it is necessary to add drives to each component. Before adding the drives, the motion states of the components are analyzed. During the conveying process, the speed of the stalk in the forward direction is consistent with the speed of the conveyor chain in the same direction. Therefore, the conveyor chain should retain the translational degree of freedom in the transport direction while restricting the other five degrees of freedom. Since there is no significant relative motion between the compression spring and the stalk in the forward direction, a fixed joint is used to anchor the fixed part of the compression spring to the ground, thereby restricting the six degrees of freedom of the fixed part. To ensure smooth startup of the conveying mechanism, the drive function for the corresponding components is initially set as STEP (time, 0, 0, 1, 900) in the transport direction. The drive is added using the same command method.

To more accurately reflect the reed stalk conveying process, collision contact forces must also be added. In ADAMS, contact forces can be calculated using two methods: the *Impact* function method and the restitution coefficient method. The *Impact* function method performs better under continuous contact conditions, so this paper uses the *Impact* function method to define the collision contact forces between the stalk and various components during the conveying process[23,24]. The expression of the *Impact* function is as follows:

$$F_{Impact}=\begin{cases}0, & x_0<x\\ k(x_0-x)^e-c_{\max}\cdot step(x,x_0-d_{\max},1,x_0,0)\cdot\left(\dfrac{dx}{dt}\right), & x\le x_0\end{cases} \tag{3}$$

In the equation: x_0 represents the initial distance between the two objects to be collided; x represents the actual distance between the two objects during the collision process; dx/dt represents the relative velocity of the two objects; k is the stiffness coefficient; e is the collision exponent; $c_{\max}$ is the damping coefficient; $d_{\max}$ is the penetration depth.

The parameter setting values of the final *Impact* function are listed in Table 1. The contact is automatically added using the "contact create" command, where the contact type between the stalk and the chain link is defined as flexible body to rigid body, and the contact type between the stalk and the compression spring is defined as flexible body to flexible body. After setting up the kinematic pairs, drives, and contacts in the reed stalk transport dynamic model, the final reed stalk-conveyor mechanism rigid-flexible coupling parametric model is shown in Figure 7.

Table 1 Impact function parameter settings

Parameters	Contact value with the chain link	Contact value with compression spring
Stiffness coefficient k/N·mm^{-1}	5.91	3.19
Collision exponent e	2.2	2.2
Damping coefficient $c_{\max}$/N·s·mm^{-1}	0.0032	0.0017
Penetration depth $d_{\max}$/mm	0.1	0.1
Coefficient of static friction	0.55	0.55
Coefficient of kinetic friction	0.28	0.28
Static translation speed/mm·s^{-1}	0.1	0.1
Friction translation speed/mm·s^{-1}	10	10

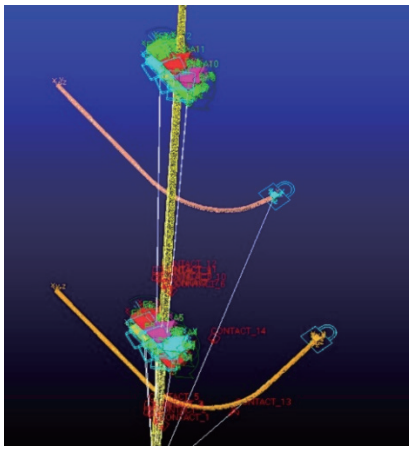

Figure 7 Rigid-flexible coupling simulation model of reed stalk and conveying mechanism

3.2.2 Optimization of structural parameters for conveyor chain links

During the conveying process of reed stalks, breakage and fracture are prone to occur. These phenomena are related to the force exerted by the conveying mechanism on the reed stalks, specifically the collision contact force between them. Therefore, the maximum contact force between the conveying mechanism and the stalk during transport is used as the experimental evaluation criterion. The specific value of this criterion is obtained by combining the Measure module's Function Builder and Range Measure functions. The influence of the chain link tooth angle and the chain link thickness on the maximum contact force is shown in Figure 8.

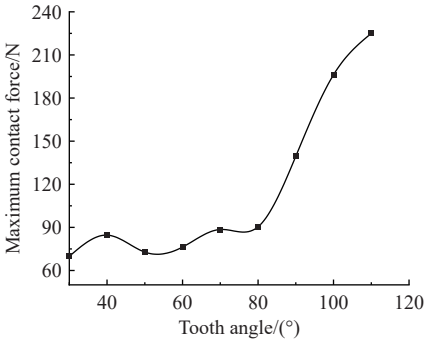

a. Relationship between tooth angle and maximum contact force

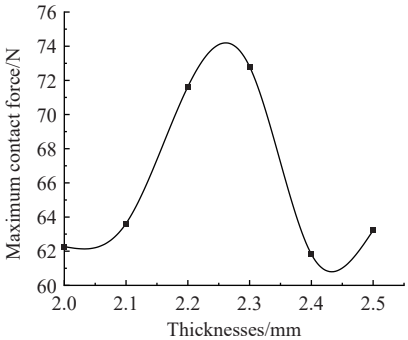

b. Relationship between thickness and maximum contact force

Figure 8 Influence of chain link structural parameters on maximum contact force

As shown in Figure 8a, when the tooth angle increases from 30° to 110°, the maximum contact force increases with the tooth angle. Therefore, a tooth angle between 30° and 60° is more suitable. Based on the analysis of the chain link structure and the results of the single-factor test on the tooth angle, the optimal value for the tooth angle is determined to be 50° under the condition of ensuring sufficient strength at the root of the tooth. As shown in Figure 8b, when the chain link thickness is 2.0 mm and 2.4 mm, the maximum contact force is relatively small. Thus, the optimal thickness of the chain link is determined to be 2.0 mm and 2.4 mm. To obtain the optimal structural parameters for the conveyor chain link, a full-factor experiment was conducted with the tooth angle and chain link thickness as the experimental factors, and the instantaneous maximum contact force as the evaluation index. The levels of the tooth angle factor were set at 45°, 50°, and 55°, while the levels of the plate thickness factor were set at 2.0 mm and 2.4 mm. After the full-factor simulation experiment, the instantaneous maximum contact force-time data during the conveying process were obtained through the ADAMS PostProcessor module. The results of the full-factor simulation experiment show that when the tooth angle is 50° and the chain link thickness is 2.0 mm or 2.4 mm, the maximum contact force is relatively small, with little difference between the two. Considering both the goal of maintaining the maximum contact force at a low level and the need to improve the overall stability of the prototype through lightweight design of the cutting platform, the final optimal structural parameters for the conveyor chain link are determined to be a tooth angle of 50° and a chain link thickness of 2.0 mm.

4 Experiment

4.1 Experimental materials

The reed stalks were collected in January 2024 from the Daxiaogang Experimental Field, Huangshagang Town, Sheyang County, Jiangsu Province, China. The height of the reed plants ranged from 3000 mm to 4500 mm, and the stalk base diameter ranged from 10 mm to 20 mm. Stalks with a diameter of approximately 13 mm, free from pests, diseases, and damage, were randomly selected as the test materials.

4.2 High-speed photography experiment

4.2.1 Experimental equipment

To further analyze the contact between the conveyor device and the reed stalks, the motion parameters during the conveying process, and the interaction between the working components, as well as to validate the theoretical analysis, high-speed photography experiments of the upright transport of reed stalks were conducted, as shown in Figure 9. Using high-speed photography technology, the motion patterns of the stalk feeding, guiding, and conveying processes were observed and analyzed. The ProAnalyst analysis system was used to calculate and analyze the motion state and trajectory of the stalks from the high-speed video. Based on this, the conveying operation mechanism was revealed, providing a theoretical basis for the parameter optimization of the conveyor device. The Faxtec HiSpec 5 high-speed camera, with a resolution of 1488 pixels × 1230 pixels, controlled by HiSpec software, was used to record the reed stalk conveying process. The camera's frame rate was set to 319 fps, with an exposure time of 3132 μs. To facilitate observation, the camera was positioned parallel to the lower conveyor chain, with the imaging field focused on the intersection of the guiding device and the lower conveyor chain, ensuring a complete view of the conveying process.

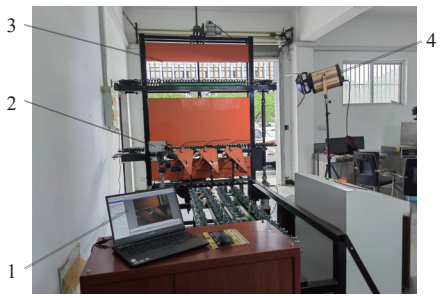

1.Computer and control system; 2.High-speed camera; 3.Test bench; 4.Photography lighting

Figure 9 High-speed photography testing scene of reed stalks

4.2.2 Conveyor high-speed photography analysis

Analysis of the upright conveying process of reed stalks shows that one operational cycle of the conveyor device includes four stages: stalk feeding, stalk guiding, clamping and conveying, and stalk detachment. The Faxtec HiSpec 5 high-speed camera was used to capture the conveying process of the reed stalks, as shown in Figure 10. The conveying process of the stalks can be divided into three stages. Figures 10a and 10b show the contact phase between the stalks and the guiding device. Under the action of the feeding device, the stalks move along the edge of the guiding plate towards the cutting table, while the reciprocating double-action knife cutting device at the lower end cuts the stalks at their base. After cutting, the stalks continue to approach the cutting table due to their inertia. As the stalks make contact with the weed-guiding star wheel, the star wheel pushes the stalks into the clamping conveyor device. It should be noted that the weed-guiding star wheel is unlikely to push the stalks into the clamping conveyor device with just one contact; the interaction between the stalk and the star wheel needs to occur multiple times. The number of interactions is jointly determined by the feeding device speed and the conveyor chain speed. Figure 10c

shows the stalk upright transport stage. Under the action of the weed-guiding star wheel, the stalk enters the clamping conveyor device, which consists of the conveyor chain, weed-guiding star wheel, and compression spring. At this stage, the compression spring and the conveyor chain form the transport channel. The stalk is laterally clamped and conveyed under the combined action of the chain's sprockets, the compression spring, and the weed-guiding star wheel. Due to the repeated contact with sprockets and the weed-guiding star wheel, which have different speeds and directions, the stalk is prone to rotational motion during the clamping and conveying process. Figure 10d shows the stalk detachment stage. The stalk is laterally conveyed to the side of the cutting table under the action of the upright conveyor device. At the end of the transport, the chain switches from horizontal motion to rotational motion. Under the action of the chain sprockets, the stalk is projected and detached from the upright conveyor device.

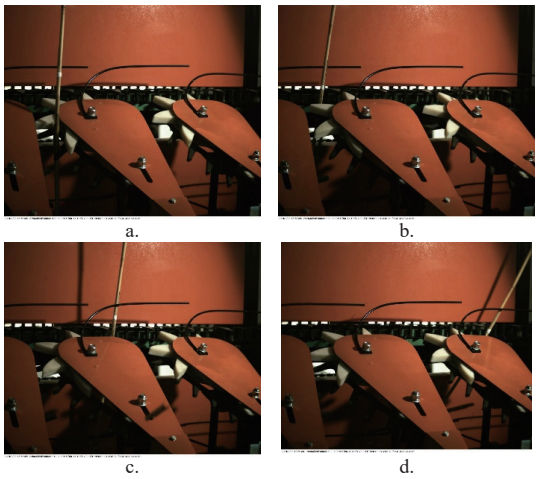

Figure 10 High-speed imaging of reed upright conveying process

To understand the influence of conveying motion parameters on operational performance, a quantitative analysis of the reed stalk conveying process was conducted using the ProAnalyst analysis system. Figure 11 shows the trajectory measurement of the marker points on the reed stalk, where the transverse conveyor speed is 1.2 m/s, and the speed ratio between the conveyor and feeding speed is 1.3. The specific measurement steps are as follows: First, two nuts mounted on adjacent guiding devices are selected as reference points in the ProAnalyst software. These two reference points are connected to set the *x*-axis, and the actual distance between the nuts is used to establish the scale ratio. Then, the marker points on the stalk are tracked frame by frame and marked with yellow points, with the moment of contact between the stalk and the guiding device being designated as the starting point (Frame 1). The time interval is 31 ms, and high-speed images are captured for each frame. Finally, the trajectory measurement origin is defined.

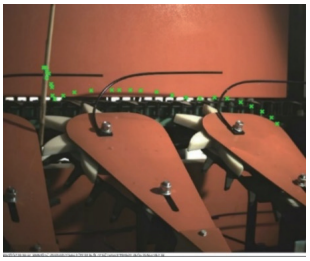

Figure 11 Trajectory measurement of marker points on reed stalk

After completing the trajectory measurement, the speed and acceleration variation curves along the *x*-axis of the reed stalk from the contact with the guiding device to the end of the conveying process were extracted, as shown in Figure 12. From the speed and acceleration variation curves, it is evident that multiple interactions occur between the conveying device and the stalk. From 0 to 0.4 s, the stalk enters the conveying device along the edge of the guiding plate with minimal speed and acceleration changes. This is primarily due to the collision between the stalk and the guiding plate. From 0.4 to 0.6 s, the interaction between the stalk and the tooth of the star wheel occurs, causing the stalk to swing left and right. Both the speed and acceleration fluctuate significantly due to the large speed difference between the stalk, which has almost zero lateral speed before contact, and the star wheel tooth, which moves at a lateral speed of 1.2 m/s. From 0.6 to 1.2 s, the stalk completely enters the gripping conveying device. Under the combined effect of the conveyor chain teeth, compression spring, and star wheel, the speed and acceleration of the stalk fluctuate within a certain range in the conveying channel. During this period, the speed of the reed stalk aligns closely with the lateral conveying speed of the chain, and the acceleration variation range becomes smaller than before. The analysis of the motion test results during stalk transportation shows that a higher chain conveying speed tends to cause large fluctuations in the stalk's speed and acceleration, leading to stalk breakage. On the other hand, a lower chain conveying speed results in the stalk falling over before it can be transported to the cutting platform within the limited time, causing a blockage in the stalk transport. Therefore, an optimal chain conveying speed is crucial for the effective transportation of the stalk.

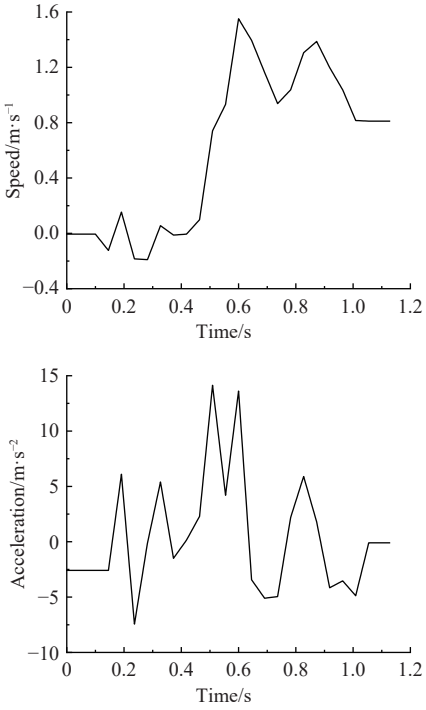

Figure 12 Speed and acceleration curves during transportation process of reed stalks

4.3 Parameter optimization experiment

4.3.1 Evaluation index

Before the experiment, the overall position of the feeding device is adjusted and fixed to ensure that the upright reed stalks enter the conveying device at an optimal position. Additionally, three asynchronous motors are used to adjust the upright movement

of the upper conveying chain, ensuring the position of the upper conveying chain meets the experimental conditions and fixing it in place, as shown in Figure 13. Since there is currently no specific standard for the harvesting quality of reed harvesters, the quality evaluation criteria refer to the standards for other stalk crop harvesters[25,26]. Ultimately, the damage rate and conveying rate are selected as the evaluation indicators for the harvesting quality of the reed conveying test stand. The damage rate refers to the ratio of damaged stalks to the total number of test stalks among the successfully conveyed stalks, while the conveying rate refers to the ratio of successfully conveyed stalks to the total number of test stalks.

1. Conveying device; 2. Test control platform; 3. Feeding device; 4. Reed stalks; 5. Three asynchronous motors

Figure 13 Reed upright conveying platform test

4.3.2 Experimental design

Based on the theoretical analysis and high-speed photography test analysis above, the experimental factors selected are the lateral conveyor speed of the chain A, the speed ratio between the lateral conveyor speed of the chain and the feeding speed B, and the position of the upper conveyor chain C. The transport damage rate H and conveying rate G are the operational performance indicators. A response surface test is designed according to the Box-Behnken Designs experimental requirements[27-29], with the experimental factors and levels as listed in Table 2. Before the experiment, the reed stalks are inserted into the fastening cylinder of the securing device, and the push plate is tightened to prevent the stalks from swaying left or right.

Table 2 Coding table of experimental factors and levels

Factor	Experimental level		
	–1	0	1
Lateral conveyor speed of chain A/m·s^{-1}	0.9	1.2	1.5
Speed ratio B	1.2	1.3	1.4
Position of upper conveyor chain C/m	1.25	1.35	1.45

4.3.3 Experimental results and analysis

The experimental plan and results are listed in Table 3. Based on the experimental results, the response parameters are analyzed and a mathematical model is established.

To determine the influence of each experimental factor and their interactions on the evaluation indicators, a quadratic regression analysis was performed on the experimental results using software, followed by multiple regression fitting. The regression equations for the damage rate H and the transport rate G were obtained, as shown in the following formulas:

$$H = 219.67 - 15.08A - 23.58B - 289.78C - 17.50AB - 25.83AC - 140.00BC + 35.78A^2 + 94.50B^2 + 184.50C^2 \quad (4)$$

$$G = -1014.30 - 24.79A - 155.26B + 1792.43C + 2.67AB + 86.83AC + 23.25BC - 43.03A^2 + 41.98B^2 - 699.53C^2 \quad (5)$$

Further analysis was conducted on the above equations, and significance tests were performed on the regression coefficients of each term. The results are listed in Table 4.

Table 3 Results and design of tests

No.	Factor level			Response value	
	Lateral conveyor speed of chain A/m·s^{-1}	Speed ratio B	Position of upper conveyor chain C/m	Damage rate H/%	Conveying rate G/%
1	–1	0	–1	13.5	84.15
2	1	1	0	20.7	85.94
3	0	–1	–1	12.2	83.28
4	0	–1	1	15.4	92.36
5	0	1	1	15.3	91.27
6	0	0	0	11.2	93.90
7	1	0	–1	23.6	75.64
8	–1	–1	0	11.3	94.55
9	1	–1	0	19.6	88.84
10	0	0	0	11.6	91.59
11	0	0	0	12.8	93.37
12	0	0	0	12.5	93.22
13	1	0	1	19.8	86.56
14	–1	1	0	14.5	91.33
15	–1	0	1	12.8	84.65
16	0	1	–1	17.7	81.26
17	0	0	0	13.7	96.01

Table 4 Regression equation analysis of variance results

Source of variation	Damage rate H				Conveying rate G			
	Sum of squares	DoF	F	p	Sum of squares	DoF	F	p
Model	216.80	9	19.98	0.0003**	475.67	9	17.49	0.0005**
A	124.82	1	103.53	<0.0001**	39.16	1	12.96	0.0087**
B	11.76	1	9.76	0.0168*	10.65	1	3.52	0.1026
C	1.71	1	1.42	0.2723	116.36	1	38.51	0.0004**
AB	1.10	1	0.91	0.3708	0.026	1	8.472×10^{-3}	0.9292
AC	2.40	1	1.99	0.2009	27.14	1	8.98	0.0200*
BC	7.84	1	6.50	0.0381*	0.22	1	0.072	0.7968
A^2	43.66	1	36.21	0.0005**	63.15	1	20.90	0.0026**
B^2	3.76	1	3.12	0.1207	0.74	1	0.25	0.6354
C^2	14.33	1	11.89	0.0107*	206.04	1	68.19	<0.0001**
Residual	8.44	7			21.15	7		
Lack of fit	4.51	3	1.53	0.3369	11.02	3	1.45	0.3539
Error	3.93	4			10.13	4		
Total	225.24	16			496.82	16		

Note: ** Extremely significant (p<0.01); * Significant (p<0.05).

From the analysis results in Table 4, it can be seen that the response surface models for damage rate H and conveying rate G have p-values of 0.0003 and 0.0005, respectively, both of which are smaller than 0.01, indicating that both models are statistically significant. The lack-of-fit values for these two indicators are 0.3369 and 0.3539, respectively, both greater than 0.05, indicating a good fit for both models. The coefficient of determination R^2 for the two models are 0.9625 and 0.9574, respectively, which suggests that the models fit the data well and the response surface analysis results are reliable. Therefore, this model can predict and analyze the changes in the operational performance of the reed stalk gripping and conveying test platform.

From the significance analysis above, it can be concluded that in the damage rate H response surface model, A and A^2 have a

highly significant impact on the model, while B, BC, and C^2 have a significant impact. In the conveying rate G response model, A, C, A^2, and C^2 have a highly significant impact, while AC had a significant impact. From the analysis, it can be seen that the influence of these three factors on the damage rate H shows a descending order of $A>B>C$, and their influence on the conveying rate G shows a descending order of $C>A>B$.

4.3.4 The influence of interactive factors on evaluation metrics

By fixing one factor at the middle level, the interaction effects of the other two factors on the evaluation indicators are analyzed. The impact of the three factors-chain lateral conveying speed, speed ratio, and the position of the upper conveyor chain on the damage rate and conveyance rate is analyzed using response surface and contour plots.

Figure 14a shows the response surface of the interaction between chain lateral conveying speed and speed ratio on the damage rate when the position of the upper conveyor chain is at the middle level, i.e., C=1.350 m. It can be observed that the interaction between these two factors is not significant, and the effect of speed ratio on the damage rate is less pronounced than that of chain lateral conveying speed. When the chain lateral conveying speed is at a low level, the damage rate will increase rapidly with the increase in speed ratio; when the chain lateral conveying speed is at a high level, the damage rate will increase slowly as the speed ratio increases. This is because at higher speed ratios, the bending angle formed by the stalk during the grain separation process is larger, and the grain separator cannot feed the reed stalks into the conveying device in time. Additionally, the large speed difference leads to more violent collisions between the reed stalk and the conveying device. Figure 14b shows the response surface of the interaction between chain lateral conveying speed and upper conveyor chain position on the damage rate when the speed ratio is at the middle level, i.e., B=1.3. It can be observed that the interaction between these two factors is not significant, and the effect of the upper conveyor chain position on the damage rate is less significant than that of the chain lateral conveying speed. When the conveying speed is at a lower level, the damage rate decreases slowly and then increases slowly with an increase in the upper conveyor chain position. When the chain lateral conveying speed is at a higher level, the damage rate decreases rapidly and then increases slowly with an increase in the upper conveyor chain position. This is because when the upper conveyor chain position is lower, the force acting on the reed stalk from the conveyor chain is primarily lower, resulting in greater force on the stalk. However, when the upper conveyor chain position is higher, the bending phenomenon during the clearing process causes the top of the stalk to tilt backward due to inertia, preventing the upper conveyor chain from effectively guiding the reed stalk into the conveying mechanism. Figure 14c shows the response surface of the interaction between speed ratio and upper conveyor chain position on the damage rate when the chain lateral conveying speed is at the middle level, i.e., A=1.20 m/s. It can be observed that the interaction between these two factors is significant, with the effect of the upper conveyor chain position on the damage rate being less significant than the effect of the speed ratio. At lower speed ratios, the damage rate decreases slowly and then increases slowly with an increase in the upper conveyor chain position. At higher speed ratios, the damage rate similarly decreases rapidly and then increases slowly with an increase in the upper conveyor chain position. This is because the increase in the upper conveyor chain position enhances the force location of the conveying chain, improving the distribution of external forces on the stalk. When the upper conveyor chain position is high enough that the distance between the conveying chain's pick-up teeth and the stalk's backward tilt during the clearing process becomes smaller than the distance the stalk moves due to its inertia, the stalk's inertial motion will no longer allow it to smoothly enter the conveying mechanism, leading to inevitable damage.

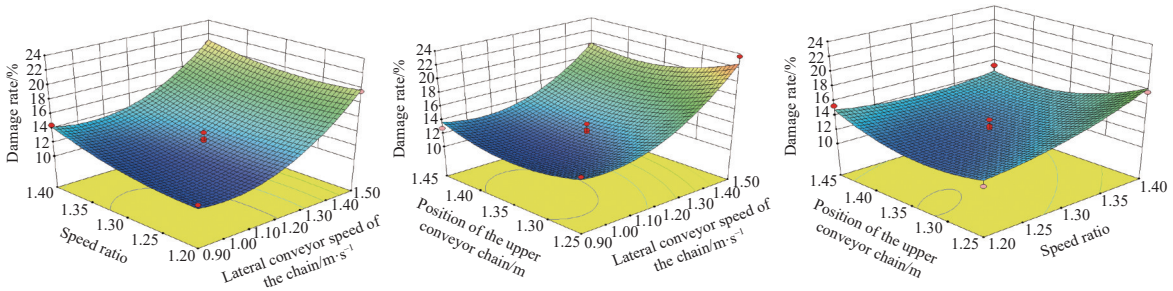

a. C=1.350 m b. B=1.3 c. A=1.20 m/s

Figure 14 Influence of interaction on damage rate

Figure 15a shows the response surface plot of the interaction between chain lateral conveyor speed and speed ratio on the conveying rate when the upper conveyor chain position is at the intermediate level, i.e., C=1.350 m. It can be seen that the interaction between these two factors is not significant, and the effect of speed ratio on conveying rate is less significant than the effect of chain lateral conveyor speed. Under the same speed ratio conditions, the conveying rate increases rapidly and then decreases with the increase in chain lateral conveying speed. This is because, initially, an increase in chain lateral conveying speed reduces the conveying time, minimizes reed stalk lodging, and facilitates conveying, resulting in a rapid increase in conveying rate. However, when the conveying speed is too high, the chain teeth form a closed surface, which hinders the reed stalks from entering the chain for conveying, leading to a decrease in the conveying rate. Figure 15b shows the response surface plot of the interaction between chain lateral conveying speed and upper conveyor chain position on the conveying rate when the speed ratio is at the intermediate level, i.e., B=1.3. It can be seen that the interaction between these two factors is significant, and the effect of upper conveyor chain position on conveying rate is more significant than the effect of chain lateral conveying speed. Under the same chain lateral conveying speed conditions, the conveying rate first increases rapidly and then decreases slowly as the upper conveyor chain position increases. This is because, initially, the increase in upper conveyor chain position raises the position of the conveying chain's acting force, which facilitates the chain teeth in pushing the upper part of the reed stalk, reducing stalk lodging and improving conveying.

However, when the upper conveyor chain position becomes too high, the force exerted by the upper chain teeth on the reed stalk becomes too strong, and since the reed stalk is softer near the top, it is less favorable for the separation of the reed stalks, resulting in a decrease in conveying rate. Figure 15c shows the response surface plot of the interaction between speed ratio and upper conveyor chain position on conveying rate when the chain lateral conveying speed is at the intermediate level, i.e., A=1.20 m/s. It can be seen that the interaction between these two factors is not significant, and the effect of upper conveyor chain position on conveying rate is more significant than the effect of speed ratio. Under the same upper conveyor chain position conditions, the conveying rate gradually decreases as the speed ratio increases. This is because as long as the chain lateral conveying speed and upper conveyor chain position are reasonable, the reed stalks can be successfully conveyed. However, the increase in speed ratio reduces the feeding speed, leading to more cycles of the star wheel, which causes some stalks to be damaged or broken, thus hindering the conveying process.

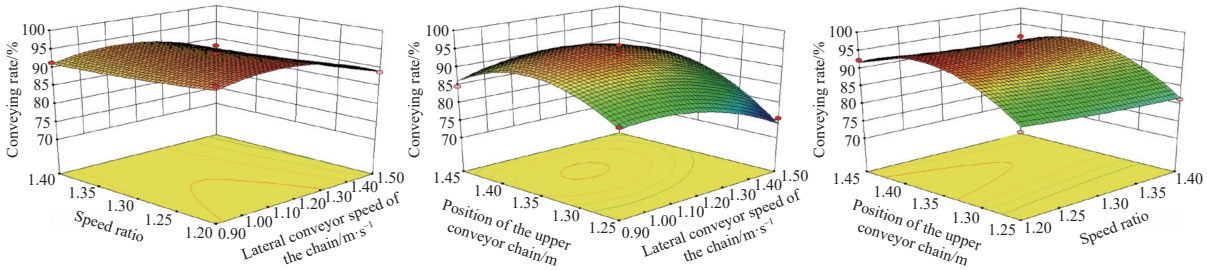

a. C=1.350 m b. B=1.3 c. A=1.20 m/s

Figure 15 Influence of interaction on conveying rate

4.4 Parameter optimization and test verification

To obtain the optimal parameter combination for the upright transport device, the Design-Expert data analysis software Optimization module was used, combined with the mathematical models for damage rate and conveying rate optimization. A multi-objective optimization was performed with the following constraints: min H, max G; 0.9 m/s≤A≤1.5 m/s, 1.2≤B≤1.4, 1.25 m≤C≤1.45 m. The optimized parameter combination obtained was: chain lateral conveyor speed of 1.10 m/s, speed ratio of 1.2, and upper conveyor chain position of 1.37 m. At this point, the model predicts a damage rate of 11.20% and a conveying rate of 95.78%.

To ensure the accuracy of the optimization results, a validation test was conducted using the above optimal parameter combination, with a chain lateral conveying speed of 1.1 m/s, a speed ratio of 1.2, and an upper conveyor chain position of 1.37 m. The validation test was repeated three times, and the average values were taken. The test results showed a damage rate of 11.90% and a transport rate of 95.11%. The experimental values of H and G showed minimal deviation from the predicted values, indicating that the optimized parameter combination is reliable.

5 Conclusions

This paper conducted an in-depth investigation of reed stalk conveying technology, revealing the mechanism of action of the stalk conveying mechanism in reed transport. It optimized the structure and motion parameters of the conveying mechanism, thereby improving the quality of the conveying operation. The main conclusions are as follows:

1) This paper presents an upright conveying device designed for a reed harvester, which mainly consists of a stalk feeding star wheel, conveying chains, compression springs, and guiding plates. It effectively addresses issues such as stalk breakage and blockages during the reed harvester conveying process.

2) Through simulation analysis of the reed stalk-conveyor device's rigid-flexible coupling model, the impact of the conveyor chain plate's structural parameters on the maximum contact force exerted on the reed stalks was determined. The optimal structural parameters for the conveyor chain plate were identified as a tooth profile angle of 50° and a chain plate thickness of 2.0 mm. High-speed photography experiments were used to capture the motion state and trajectory of the reed stalks, revealing that the cause of breakage and blockages during reed stalk conveyance was the high fluctuation in speed and acceleration at higher chain speeds, which led to stalk breakage. On the other hand, lower chain speeds caused the stalks to fall over before reaching the cutter bar side within the limited time, resulting in blockages in the stalk-guiding device.

3) A dual-objective optimization was performed using the established mathematical model for predicting the quality of the conveying operation. The optimal parameter combination for the upright conveying device was determined to be a chain lateral conveying speed of 1.1 m/s, a speed ratio of 1.2, and an upper conveyor chain position of 1.37 m. The experimental results showed a damage rate of 11.90% and a conveying rate of 95.11%, with all operational indicators meeting the requirements for mechanized reed harvesting and conveying operations.

Future research will focus on further optimizing the reed upright conveying test bench rig by adding adjustable factors such as conveying chain vibration and spring elasticity. In addition, the theoretical model will be enhanced to account for the uneven distribution of reed stalks and to introduce some random factors to more realistically reflect the actual conveying process.

Acknowledgements

The research work was supported by Special Funds for Jiangsu Province Agricultural Science and Technology Independent Innovation Fund Project (Grant No. CX3096) and the Agricultural Science and Technology Innovation Program of Chinese Academy of Agricultural Sciences (Grant No. 31-NIAM-05).

[References]

[1] Xu J, Li Y, Feng K P, Xie J X, Wang Y S, Zhang Z Q. Study on degradation properties of poly (lactic acid)/reed fiber composites. China Plastics, 2023; 37(4): 23–29. (in Chinese)

[2] Wen Z W, Liu F Y, Cui X J, Zhang G, Meng W H, Xie J X, et al. Mechanical modification of polylactic acid with reed fibers for flame-retardant application. China Plastics, 2021; 35(11): 38–43. (in Chinese)

[3] Jian Y, Fan X E, Qiu B Y, Tian X D, Yang X. Preparation and microwave absorption properties of ferrite/reed charcoal composites. Acta Materiae Compositae Sinica, 2024; 41(10): 5351–5360. (in Chinese)

[4] Song Z F, Shi X Q, Liu Z, Sun D, Cao N, Mo Y K, et al. Synthesis and characterization of reed-based biochar and its adsorption properties for Cu^{2+} and bisphenol A (BPA). Environmental Chemistry, 2020; 39(8): 2196–2205. (in Chinese)
[5] An C W, Li S J, Liu T, Liu M H. Effect of AMF and PGPR combined with phragmites australis on the remediation of heavy metal polluted river sediment. Journal of Safety and Environment, 2024; 24(9): 3606–3616. (in Chinese)
[6] Yu J H, Wang L H, Kang D J, Zheng G Y, Guo B L, Zhong J C, et al. Temporal changes in fractions and loading of sediment nitrogen during the holistic growth period of phragmites australis in littoral Lake Chaohu, China. Journal of Lake Sciences, 2021; 33(5): 1467–1477. (in Chinese)
[7] Ji K Z, Li Y M, Ji B B, Liang Z W, Du T. Discrete element method used to analyze the operating parameters of the cutting table of crawler self-propelled reed harvester. INMATEH–Agricultural Engineering, 2023; 71(3): 345–355.
[8] Yin Q, Li Y M, Ji B B, Chen L P. Design and experiment of clamping and conveying device for self-propelled reed harvester. Journal of Agricultural Mechanization Research, 2023; 45(4): 113–118. (in Chinese)
[9] He H P, Shen C, Li X W, Zhang B, Chen Q M, Huang J C, et al. Status and prospect of reed harvesting equipment in China. International Agricultural Engineering Journal, 2019; 28(3): 128–136.
[10] Liu J B, Song X, Liu Y L, Guo J W, Li Y C, Lv H Y. Experimental study on mechanized harvesting of phragmites communis in Baiyang Lake. Journal of Agricultural Mechanization Research, 2023; 45(1): 196–200. (in Chinese)
[11] Chen M J, Guo W, Qu H L, Ping Y H, Chen Y S. Current situation and development proposals of reed harvesting equipment in China. Journal of Chinese Agricultural Mechanization, 2013; 34(4): 29–31, 41. (in Chinese)
[12] Poulin B, Lefebvre G, Allard S, Mathevet R. Reed harvest and summer drawdown enhance bittern habitat in the Camargue. Biological Conservation, 2009; 142(3): 689–695.
[13] Ivan G, Vladut V, Ciuperca R, Moise V. Kinematic scheme of equipment to reed harvesting machine MRS. 16th International Scientific Conference: Engineering for Rural Development, 2017; pp.841–847. DOI: 10.22616/ERDev2017.16.N171.
[14] Ji B B, Li Y M, Xu L Z, Yin Q. Reed harvesting technology and equipment. Agricultural Engineering, 2021; 11(6): 11–16. (in Chinese)
[15] Huang J C, Zhang B, Tian K P, Liu H L, Shen C. Design and optimization of the parameters of the key components for reed harvester. Int J Agric & Biol Eng, 2022; 15(6): 96–103.
[16] Wang Y X. Engineering application manual for conveyor chain and special chain. Beijing: China Machine Press, 2000. (in Chinese)
[17] Guo X X, Zhang D L, Bu L X, Cui M, Wang L X. Design and analysis on gripping delivery mechanism for vertical-roll type of corn harvester. Journal of Agricultural Mechanization Research, 2015; 37(2): 124–127. (in Chinese)
[18] Wang X S. Design and experiment of 4SY-2.0 self-propelled rape. Master dissertationHunan Agricultural University, 2016; 95p.(in Chinese)
[19] Huang J C, Tian K P, Shen C, Zhang B, Liu H L, Chen Q M, et al. Design and parameters optimization for cutting-conveying mechanism of ramie combine harvester. Int J Agric & Biol Eng, 2020; 13(6): 94–103.
[20] Jin C Q, Yin W Q, Wu C Y. Development and experiment of rape windrower transportation device with poke finger conveyor chain. Transactions of the CSAE, 2013; 29(21): 11–18. (in Chinese)
[21] Cui T, Liu J, Zhang D X, Shi S. Flexible body simulation for corn stalk based on ANSYS and ADAMS. Transactions of the CSAM, 2012; 43(S): 112–115. (in Chinese)
[22] Li H T, Wu C Y, Mu S L, Guan Z H, Jiang T. Formation mechanism of laying angle of vertical rape windrower based on ANSYS-ADAMS. Transactions of the CSAE, 2020; 36(14): 96–105. (in Chinese)
[23] Chen H T, Dun G Q. Optimization of parameters for soybean lifter based on dynamic simulation of virtual prototype. Transactions of the CSAE, 2012; 28(18): 23–29. (in Chinese)
[24] Shi Y Y, Chen M, Wang X C, Zhang Y N, Odhiambo M O. Dynamic simulation and experiments on artemisia selengensis orderly harvester cutter. Transactions of the CSAM, 2017; 48(2): 110–116. (in Chinese)
[25] Liao K, Gu Q Y, Gao Z C, Xiang M Y, Tang T, Min S H, et al. Development fo reed shoot harvesters. Transactions of the CSAE, 2021; 37(15): 20–30. (in Chinese)
[26] Wang F C, Zhou X J, Shi Q X, Liu S D, Ni C A, Yao L L. Parameters study on transverse transport of new corn combine. Journal of Agricultural Mechanization Research, 2010; 32(5): 152–155. (in Chinese)
[27] Xu X H, He M Z. Experimental design and application of Design-Expert SPSS. Beijing: Science Press Co., Ltd, 2010. (in Chinese)
[28] Gu F W, Zhao Y Q, Hu Z C, Shi L L, Wu F, Xu H B, et al. Operation analysis and parameter optimization of the conveying device for uniform crushed straw throwing and seed-sowing machines. Int J Agric & Biol Eng, 2023; 16(6): 28–36.
[29] Jiang D L, Yan L M, Chen X G, Mo Y S, Yang J C. Design and experiment of nail tooth picking up device for strip type residual film recycling and baling machine. Int J Agric & Biol Eng, 2023; 16(6): 85–96.